arXiv:1105.1130v2 [hep-ph] 6 Jul 2011

Analysis of matter suppression in collective neutrino oscillations during the supernova accretion phase

Sovan Chakraborty,[1] Tobias Fischer,[2,3] Alessandro Mirizzi,[1] Ninetta Saviano,[1] and Ricard Tomàs[1]

[1] *II Institut für Theoretische Physik, Universität Hamburg, Luruper Chaussee 149, 22761 Hamburg, Germany*

[2] *GSI, Helmholtzzentrum für Schwerionenforschung GmbH, Planckstraße 1 64291 Darmstadt, Germany*

[3] *Technische Universität Darmstadt, Schlossgartenstraße 9, 64289 Darmstadt, Germany*

The usual description of self-induced neutrino flavor conversions in core collapse supernovae (SNe) is based on the dominance of the neutrino density n_ν over the net electron density n_e. However, this condition is not met during the post-bounce accretion phase, when the dense matter in a SN is piled up above the neutrinosphere. As recently pointed-out, a dominant matter term in the anisotropic SN environment would dephase the flavor evolution for neutrinos traveling on different trajectories, challenging the occurrence of the collective behavior in the dense neutrino gas. Using the results from recent long term simulations of core-collapse SN explosions, based on three flavor Boltzmann neutrino transport in spherical symmetry, we find that both the situations of complete matter suppression (when $n_e \gg n_\nu$) and matter-induced decoherence (when $n_e \gtrsim n_\nu$) of flavor conversions are realized during the accretion phase. The matter suppression at high densities prevents any possible impact of the neutrino oscillations on the neutrino heating and hence on the dynamics of the explosion. Furthermore, it changes the interpretation of the Earth matter effect on the SN neutrino signal during the accretion phase, allowing the possibility of the neutrino mass hierarchy discrimination at not too small values of the leptonic mixing angle θ_{13} (i.e. $\sin^2\theta_{13} \gtrsim 10^{-3}$) .

PACS numbers: 14.60.Pq, 97.60.Bw

I. INTRODUCTION

Massive star explosions are an active subject of research, in terms of core-collapse supernova (SN) models. The supernova problem is related to the revival of the stalled bounce shock, which forms when the collapsing stellar core reaches nuclear matter density and bounces back. It propagates out of the core and stalls on its way out due to the continuous energy loses via neutrino emission and dissociation of heavy nuclei. Independently from the explosion mechanism (see, e.g. [1–7]) the total energy emitted in neutrinos (ν) and antineutrinos ($\bar{\nu}$) during a SN is of the order of several 10^{53} erg, which makes a SN the most powerful neutrino source in the Universe. The total duration of the neutrino emission, known as the neutrino burst, can last up to 30 seconds. This ν signal represents a powerful tool to probe fundamental neutrino properties as well as the dynamics of the explosion [8].

The role of astrophysical messengers played by neutrinos during a stellar collapse is largely associated with the signatures imprinted on the observable SN neutrino burst by weak processes and flavor conversions occurring deep inside the star. In the last few years, it has been understood that the description of neutrino flavor conversions in supernovae, based on the only Mikheyev-Smirnov-Wolfenstein (MSW) effect with the ordinary matter [9], was incomplete. In particular, in the deepest supernova regions the neutrino density is so high that the neutrino-neutrino interactions dominate the flavor changes. Even if the important role played by the neutrino-neutrino interactions for the flavor evolution in supernovae was pointed out since a long time ago [10–14], only recently the first numerical experiments have been performed to characterize realistically these effects [15, 16]. These seminal investigations have stimulated a still streaming torrent of activities (see, e.g. [17], for a recent review). The general result of these studies is that neutrino-neutrino interactions create a large potential for the neutrinos, which causes large and rapid conversions between different flavors. The transitions occur collectively, i.e. in a coherent fashion, over the entire energy range. The most important observational consequence of ν–ν interactions is a swap of the ν_e and $\overline{\nu}_e$ spectra with the non-electron ν_x and $\overline{\nu}_x$ spectra in certain energy ranges [16–34].

The basic idea behind the self-induced neutrino oscillations in supernovae is that these can produce significant flavor conversions close to the ν decoupling region (i.e., at small radii) even in the presence of a large matter density [15, 35]. This would have inhibited any possible flavor transition, far from the MSW resonances (i.e., far outside the neutrino-matter decoupling region) at larger radii [36]. Subsequently, it has been realized in [37], and then confirmed in [38], that this original idea was only in part true since the matter density cannot be arbitrarily large before it affects collective flavor conversions after all. Indeed, for the strongly anisotropic emission of neutrinos streaming-off the SN core, the matter effect is trajectory dependent, inducing different oscillation phases for neutrinos traveling in different directions. When the neutrino-neutrino interaction is sufficiently strong, it forces neutrinos reaching the same position from different paths to have the same oscillation phase, overcoming the trajectory-dependent dispersion induced by the matter. Conversely, when the electron density n_e significantly exceeds the neutrino density n_ν, it has been shown that the large phase dispersion induced by the matter would sup-

press the collective phenomena. Depending on the electron density, the matter suppression can be complete, when $n_e \gg n_\nu$, or partial when the matter domination is less pronounced. Finally, when $n_e \gtrsim n_\nu$, the interference of the two comparable effects would lead to the decoherence of the collective neutrino flavor changes, producing an equal mixture between the oscillating electron and non-electron neutrino species [37].

Most of the numerical simulations of the self-induced flavor conversions in SN explosions have been focused on the late times cooling phase (at post-bounce times $t_{pb} \gtrsim 1$ s), when the matter potential is smaller than the neutrino-neutrino potential. In such a situation, collective oscillations would develop without any matter hindrance [16, 18, 31, 32]. During the earlier phase before the onset of an explosion, which is determined by mass accretion ($t_{pb} \lesssim 0.5$ s), the electron density is not negligible with respect to the neutrino density, as one can infer from the following back–of–the–envelope calculation. Given the mass accretion rate

$$\dot{m} = \frac{\partial m}{\partial r} v = 4\pi \rho r^2 v \ , \tag{1}$$

in terms of the the rest-mass density ρ at radius r, and of the matter velocity v, one gets

$$\rho \sim 10^8 \, \frac{\rm g}{\rm cm^3} \left(\frac{\dot{m}}{0.4 \ {\rm M}_\odot/s}\right) \left(\frac{10^2 \ {\rm km}}{r}\right)^2 \left(\frac{10^4 \ {\rm km/s}}{v}\right), \tag{2}$$

for typical values in the region ahead the shock-wave. Then, the net electron density at $r \sim 10^2$ km can be estimated as

$$n_e = \rho Y_e / m_B \sim 10^{32} \ {\rm cm}^{-3} \ , \tag{3}$$

where the electron fraction $Y_e \simeq 0.5$ and m_B is the nucleon mass. On the other hand, during the accretion phase, where the charged-current reactions dominate, the far-distance electron (anti)neutrino luminosities can be expressed via the change of the gravitational potential at the neutrinosphere [1] with radius r_ν as follows,

$$L_{\nu_e,\bar{\nu}_e} = \left. \frac{Gm}{r} \, \dot{m} \right|_{r_{\nu_e,\bar{\nu}_e}}$$

$$\sim 10^{52} \, \frac{\rm erg}{\rm s} \left(\frac{m}{1.5 \ {\rm M}_\odot}\right) \left(\frac{\dot{m}}{0.4 \ {\rm M}_\odot/s}\right) \left(\frac{10^2 \ {\rm km}}{r}\right). \tag{4}$$

Therefore, the neutrino particle flux $F_{\nu_e,\bar{\nu}_e} = L_{\nu_e,\bar{\nu}_e}/\langle E_{\nu_e,\bar{\nu}_e}\rangle \sim 10^{57}$ s^{-1}, for $\langle E_{\nu_e,\bar{\nu}_e}\rangle = 11$ MeV, implying

$$n_{\nu_e,\bar{\nu}_e} = \frac{F_{\nu_e,\bar{\nu}_e}}{4\pi r^2} \sim 10^{31} {\rm cm}^{-3} \ , \tag{5}$$

at $r \sim 10^2$ km. From this simple estimation, n_ν can be smaller or on the same order than n_e and hence we cannot a-priori assume that $n_e \ll n_\nu$ holds during the post-bounce accretion phase. This result is confirmed by many different SN simulations [39–42]. It is a generic feature that applies generally to core collapse SNe of massive iron-core progenitors. As an important consequence, it is not guaranteed a priori that the results of the neutrino flavor evolution obtained during the cooling phase, could be directly applied to the accretion.

The post-bounce accretion phase, where the neutrino fluxes are large, represents a particularly interesting scenario for detecting signatures of neutrino flavor transformations. Indeed, also the flavor-dependent flux differences are large with a robust hierarchy for the neutrino number fluxes, $F_{\nu_e} > F_{\overline{\nu}_e} \gg F_{\nu_x}$, where ν_x indicates the non-electron flavors. In such a situation, if dense matter effects are neglected and the flavor asymmetries are enough to prevent multi-angle effects [43], the self-induced flavor oscillations seemed to have a clear outcome, producing a complete exchange of the electron and non-electron flavors for almost all antineutrinos in the inverted neutrino mass hierarchy (IH, $\Delta m^2_{\rm atm} = m^2_3 - m^2_{1,2} < 0$) and a spectral split in the energy distributions of the neutrinos [18]. In the normal neutrino mass hierarchy (NH, $\Delta m^2_{\rm atm} > 0$), they would leave the neutrino spectra unaffected. How this picture would change if the effect of the dense matter is included, is subject of investigation of the present article. It develops and clarifies the results recently presented in our [44].

We take as benchmark the results of the recent long-term SN simulations from Ref. [7], to characterize the SN neutrino signal as well as the matter density profile evolution. We consider three cases corresponding to different supernova progenitor masses, the 8.8 M$_\odot$ O-Ne-Mg-core and the 10.8 M$_\odot$ and 18.0 M$_\odot$ iron-cores. For these three cases we find that the matter density is always larger than or comparable to the neutrino density, during the accretion phase. This finding suggests the possible hindrance (or decoherence) of collective neutrino flavor transitions for matter densities higher than (or comparable with) the neutrino densities during the accretion phase.

The plan of our paper is the following. In Section II we describe the original supernova neutrino emission during the accretion phase and in Section III we introduce the schematic supernova neutrino model we use to characterize the ν emission geometry, the neutrino potentials and the different radial ranges where self-induced oscillations and matter effects are relevant. The results of our analysis on matter suppression for the three different SN progenitor masses are presented in Section IV and the impact of the dense matter suppression on the interpretation of the Earth matter effect on the SN neutrino burst is discussed in Section V. Finally, we close with comments of our results and the conclude in Section VI.

[1] The neutrinospheres are the neutrino energy and flavor dependent spheres of last scattering.

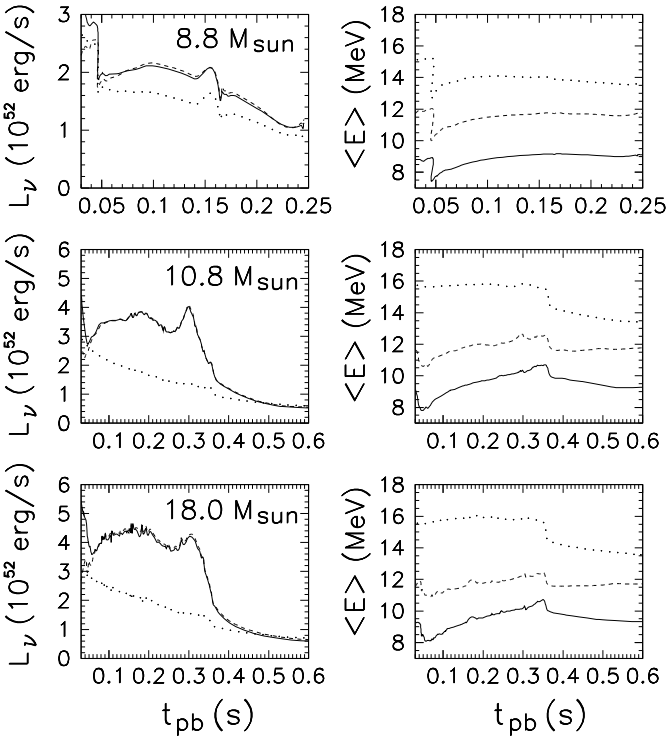


FIG. 1: Neutrino luminosities (left panels) and average energies (right panels) for the core-collapse SN simulations considered, where we distinguish ν_e (continuous line), $\bar{\nu}_e$ (dashed line) and ν_x (dotted line). The three cases are shown corresponding to different values of the supernova progenitor mass: 8.8 $M_\odot$ (top), 10.8 $M_\odot$ (middle) and 18.0 $M_\odot$ (bottom).

II. NEUTRINO SIGNAL FROM CORE-COLLAPSE SUPERNOVA EXPLOSIONS

We investigate core-collapse supernova simulations of massive progenitor stars of 8.8, 10.8 and 18 $M_\odot$. The first one belongs to the class of O-Ne-Mg-core progenitors [45, 46] and represents the threshold between thermonuclear explosions and core-collapse supernovae [4, 7]. The latter two are iron-core progenitors [47]. All models were evolved consistently through core collapse, bounce and the early post-bounce phase up to several seconds after the onset of explosion [7]. The core-collapse model is based on general relativistic radiation hydrodynamics that employs three flavor Boltzmann neutrino transport in spherical symmetry and a sophisticated equation of state for hot and dense nuclear matter [48] (for details about the supernova model, see [7, 49] and references therein). Explosions of massive iron-core progenitors cannot be obtained in spherically symmetric supernova models. In order to trigger the explosions for the 10.8 and 18 $M_\odot$ progenitor models, the heating rates are artificially enhanced in the gain region where neutrinos deposit energy in order to revive the stalled bounce shock.

Fig. 1 shows the evolution of the neutrino luminosities L_{ν_α} (left panels) and average energies $\langle E_{\nu_\alpha}\rangle$ (right panels), during the post-bounce accretion phase for all models under investigation. Here, $\nu_\alpha = (\nu_e, \overline{\nu}_e, \nu_x)$ where ν_x indicates both (μ,τ)-neutrinos and antineutrinos. The large electron flavor neutrino luminosities $\mathcal{O}(10^{52})$ erg/s are due to the continuous mass accretion at the neutrinospheres, where the electron flavor neutrino luminosities are dominated by the charged current reactions. The slightly larger $\overline{\nu}_e$ luminosity over the ν_e luminosity and the magnitude of the differences obtained in the models discussed here, is an active subject of research and may change slightly applying improved weak rates and multi-dimensional supernova models. The increasing and decreasing electron flavor luminosities reflect the propagating bounce shock (and the mass accretion rate at the neutrinospheres), which contracts and expands accordingly during the accretion phase driven by neutrino heating/cooling. Since muonic charged current processes are suppressed, $\nu_{\mu/\tau}$'s are produced only after bounce via pair-processes and the (μ/τ)-neutrino luminosities are generally smaller than the electron flavor neutrino luminosities. For the average energies, the following hierarchy holds $\langle E_{\nu_e}\rangle < \langle E_{\bar{\nu}_e}\rangle < \langle E_{\nu_x}\rangle$ for all models under investigation during the accretion phase. Furthermore, the average energies rise continuously for all neutrino flavors during the accretion phase illustrated in Fig. 1 (right panels).

After the onset of explosion, when mass accretion vanishes, the situation changes. The luminosities and average energies of all flavors decrease on a longer timescale on the order of seconds. For the O-Ne-Mg-core, we consider the neutrino signal only up to $t_{\rm pb}$=0.25 s (top panel of Fig. 1). Note that mass accretion at the neutrinospheres vanishes already at about $t_{\rm pb}$=0.03 s. This determines the onset of the explosion for this low-mass progenitor. For the 10.8 and 18 $M_\odot$ progenitor models discussed here, we show the neutrino signal up to $t_{\rm pb}$=0.6 s. For these cases, the onsets of explosion occur at about $t_{\rm pb}$=0.36 s, due to the more massive envelopes surrounding the iron-core that lead to a more extended accretion (and hence neutrino heating) phase. Note the sharp drop of the luminosities and average energies of all neutrino flavors in Fig. 1 after the onsets of explosion. These are due to the sudden flip of matter velocities from infall to expansion when the explosion shock passes through the distance of 500 km, where the observables are measured in a co-moving frame of reference. We note further that these results suggest lower average energies than often assumed in the literature [50] and a less pronounced spectral hierarchy, in particular during the later proto-neutron star cooling phase. The results obtained for the low mass O-Ne-Mg-core collapse supernova explosion and long term simulation of the proto-neutron star cooling phase, are in qualitative and quantitative good agreement with recent simulations performed by the Garching-group [51].

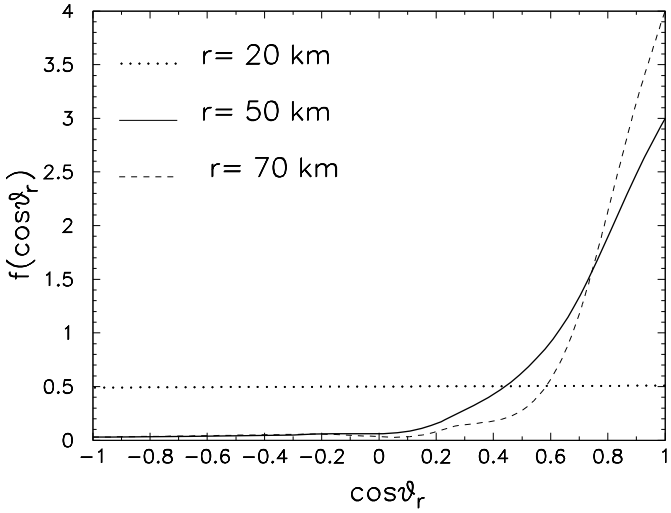


FIG. 2: 10.8 $M_\odot$ progenitor mass. Angular distributions for ν_e at $t_{\rm pb}$=0.4 s for $E_{\rm rms}$ = 11.5 MeV at different radii: r=20 km (dotted line), r=50 km (continuous line), r=70 km (dashed line).

III. SCHEMATIC SUPERNOVA MODEL

We present here our schematic assumptions to characterize the flavor conversions during the accretion phase. In particular, we describe our model for the SN neutrino emission geometry, the neutrino number fluxes of different flavors, the neutrino-neutrino and matter potentials and the different oscillation regimes.

A. Neutrino emission geometry

We assume a spherically symmetrical source ("SN core") that emits neutrinos and antineutrinos like a blackbody surface, from a neutrinosphere at radius $r = r_\nu$. We define r_ν to be the radius where the neutrino radiation field is assumed to be "half-isotropic", i.e. all outward-moving angular modes are equally occupied [43]. We remind that this conventional definition of the neutrinosphere, used in the context of the neutrino flavor conversions, is only intended to fix a boundary condition for the subsequent flavor evolution. We assume that weak processes take place at higher densities inside the neutrino-matter decoupling sphere and are negligible outside the decoupling sphere where neutrino oscillations can occur. The half-isotropic definition for the decoupling spheres does not necessarily coincide with the definition of the neutrinosphere as neutrino last scattering surface, defined as the radius where the optical depth becomes 2/3. However, in the context of collective oscillations which start at radii much larger than the assumed boundary, neutrinos are safely in a free-streaming regime [31]. Therefore, we do not have to worry about the details of the ν decoupling.

Instead of choosing arbitrarily the neutrinosphere radius, we fix it consistently with the SN simulations which provide the angular distributions of the different neutrino species as a function of time and energy at different radii. For definiteness, we have taken the ν_e's distribution as representative for all the different flavors, since electron neutrinos reach the free-streaming regime at larger radii compared to the other neutrino species during the accretion phase. The angular distributions are functions of the energy. For definiteness, we consider as reference the root mean square (rms) energy relevant for the average neutrino-nucleon interaction rates, that determine the neutrino angular distributions. As an example, in Fig. 2 we plot the ν_e angular distribution $f(\cos\theta_r) = dn_\nu/d\cos\theta_r$, where θ_r is the zenith angle of a given mode relative to the radial direction at distance r. We consider $E_{\rm rms} = 11.5$ MeV at three different radii at the post-bounce time $t_{\rm pb} = 0.4$ s, taken form the 10.8 $M_\odot$ model. As expected, at small radii ($r = 20$ km in the Fig. 2) the angular distribution is isotropic since neutrinos are in a trapping regime. They are isotropically emitted in all directions. At large radii ($r = 70$ km in the Fig. 2), neutrinos are free-streaming and their angular distribution becomes forward peaked. We schematically *assume* as neutrinosphere radius, the one at which the ν_e's angular distribution has no longer significant backward flux, i.e. a few % of the total one (at $r = 50$ km in the Fig. 2). Even if there the real angular distribution is not half-isotropic, we assume it to characterize the further flavor evolution. For our purpose of evaluating the impact of the matter effects on the self-induced flavor conversions, this simplified choice is conservative. Indeed, the real angular distributions, which are more forward-peaked than what we are assuming, would reduce the real strength of the neutrino-neutrino potential with respect to what we are assuming.

We stress that this procedure for fixing the neutrinosphere has to be taken only as an empirical prescription. However, we performed several neutrino flavor oscillation analysis changing by a factor of three the neutrinosphere radius. We find that the results on matter effects remained basically unchanged, indicating a weak dependence of the oscillation analysis from the decoupling region.

B. Neutrino number fluxes for different flavors

The neutrino particle flux for the different flavors is defined as follows $F_{\nu_\alpha} = L_{\nu_\alpha}/\langle E_{\nu_\alpha}\rangle$. In order to characterize the flux asymmetries among the different ν species we introduce the parameter [43]

$$\epsilon = \frac{F_{\nu_e} - F_{\overline{\nu}_e}}{F_{\overline{\nu}_e} - F_{\overline{\nu}_x}} \ , \qquad (6)$$

where we assume $F_{\nu_x} = F_{\overline{\nu}_x}$.

In Fig. 3 we show the neutrino number flux F_{ν_α} (left panels) and asymmetry parameter ϵ (right panels) for the three benchmark SN simulations based on the different

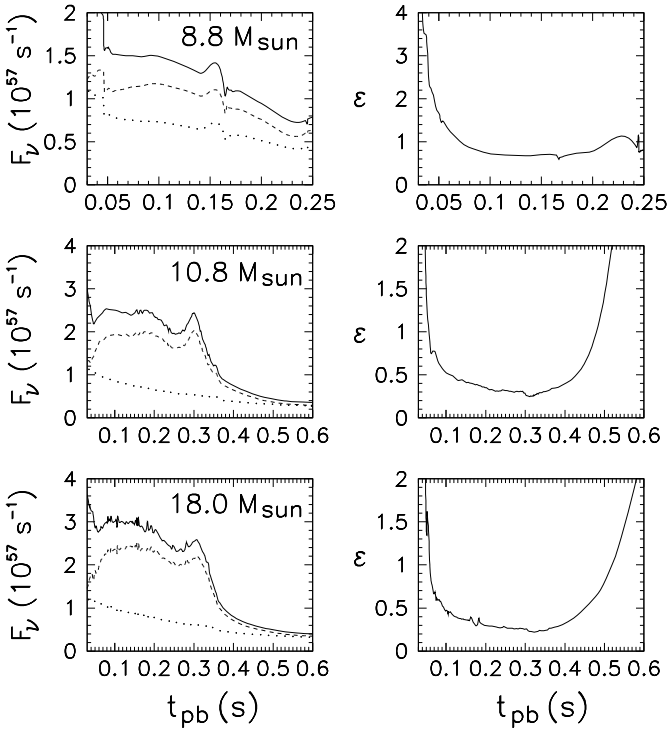


FIG. 3: Neutrino particle fluxes (left panels) and flavor asymmetry parameter ϵ (right panels) for ν_e (continuous line), $\overline{\nu}_e$ (dashed line), ν_x (dotted line).

progenitor models. The particle fluxes present the expected hierarchy, $F_{\nu_e} > F_{\overline{\nu}_e} \gg F_{\nu_x}$, during the accretion phase. The first part of the hierarchy is caused by the deleptonization of the collapsed stellar core whereas the second is due to the absence of charged-current interactions for neutrino species other than ν_e and $\overline{\nu}_e$. As a consequence of this hierarchy, the electron and non-electron neutrino particle fluxes differ by almost a factor of two during the accretion phase. Conversely, flux differences tend to become much smaller during the cooling of the SN remnant.

Passing to the asymmetry parameter ϵ [Eq. (6)], the strong excess of ν_e's during the early post-bounce deleptonization ($t_{\rm pb} \lesssim 0.05$ s), increases $\epsilon \gg 1$. Then, ϵ drops and reaches values between 0.3-0.5 during the accretion phase (see Fig. 3). After that, since the flux difference $F_{\overline{\nu}_e} - F_{\overline{\nu}_x}$ drops more rapidly than $F_{\nu_e} - F_{\nu_x}$, ϵ rises again and becomes larger than 1 for the iron-core SNe. We will see that this behavior will have important consequences on the development of the self-induced flavor conversions.

C. Non-linear neutrino flavor mixing

Our description of the non-linear neutrino flavor conversions is based on the two-flavor oscillation scenario, driven by the atmospheric mass-square difference $\Delta m^2_{\rm atm} \simeq 2.6 \times 0^{-3}$ eV^2 and by a small (matter suppressed) in-medium mixing $\theta_{\rm eff} = 10^{-3}$ [52, 53]. Three-flavor effects, associated with the solar sector, are small for the neutrino flux ordering expected during the accretion phase [32, 54].

In the normal mass hierarchy and for the spectral ordering of the accretion phase, no self-induced flavor conversion will occur and thus dense matter cannot produce any sizable new effect. Therefore, in the following we will always refer to the inverted mass hierarchy case.

The impact of the non-isotropic nature of neutrino emission on the self-induced flavor conversions is taken into account by "multi-angle" simulations [16], where one follows a large number [$\mathcal{O}(10^3)$] of neutrino trajectories. The ν's emitted from a SN core naturally have a broad energy distribution. However, this is largely irrelevant for our purposes, since large matter effects would lock togheter the different neutrino energy modes, both in case of supression [37] and of decoherence [43] of collective oscillations. Therefore, to simplify the complexity of the numerical simulations, we assume all ν's to be represented by a single energy, that we take $E = 15$ MeV. This approximation is reasonable since our main purpose is to determine if the dense matter affects the development of the self-induced transformations. This choice results in the neutrino vacuum oscillation frequency

$$\omega = \left\langle \frac{\Delta m^2_{\rm atm}}{2E} \right\rangle = 0.4 \ \ {\rm km}^{-1} \ . \qquad (7)$$

The strength of the neutrino-neutrino interaction, normalized at the neutrinosphere, is parametrized by [43]

$$\begin{aligned} \mu_r &= \sqrt{2} G_F \left[n_{\overline{\nu}_e}(r) - n_{\overline{\nu}_x}(r) \right] \\ &= 7 \times 10^5 \ \ {\rm km}^{-1} \left(\frac{L_{\overline{\nu}_e}}{\langle E_{\overline{\nu}_e} \rangle} - \frac{L_{\overline{\nu}_x}}{\langle E_{\overline{\nu}_x} \rangle} \right) \\ &\times \ \frac{15 \ \ {\rm MeV}}{10^{52} {\rm erg}} \left(\frac{10 \ \ {\rm km}}{r} \right)^2 \qquad (8) \end{aligned}$$

where $n_{\nu_\alpha}(r)$ is the flux of the neutrino species ν_α at radius r (for a definition of n_{ν_α}, see Eq.(5)). The matter potential is represented by [36]

$$\begin{aligned} \lambda_r &= \sqrt{2} G_F n_e(r) = 1.9 \times 10^6 \ \ {\rm km}^{-1} \\ &\times \ \left(\frac{Y_e}{0.5} \right) \left(\frac{\rho}{10^{10} \ \ {\rm g/cm}^3} \right) \qquad (9) \end{aligned}$$

encoding the net $n_e \equiv n_{e^-} - n_{e^+}$ electron density, where $Y_e = Y_{e^-} - Y_{e^+}$ is the net electron fraction and ρ is the matter density. The neutrino term μ_r declines always as r^{-2} due to the geometric dilution outside the decoupling spheres, whereas λ_r is given by the detailed matter profile from the SN simulations.

D. Oscillation regimes

In the absence of matter suppression, collective neutrino flavor transformations will start outside the syn-

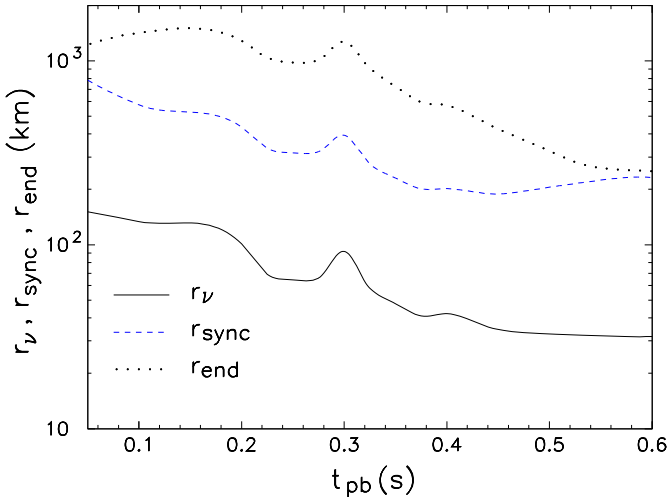


FIG. 4: 10.8 $M_\odot$ progenitor mass. Time evolution of r_ν (continuous line), $r_{\rm sync}$ (dashed curve) and $r_{\rm end}$ (dotted curve).

chronization radius, given by [43]

$$\frac{r_{\rm sync}}{r_\nu} = \left(\frac{\sqrt{1+\epsilon}-1}{2}\right)^{1/2} \left(\frac{\mu_r\big|_{r=r_\nu}}{\omega}\right)^{1/4} , \qquad (10)$$

and are expected to develop at least until radii when the neutrino-neutrino interaction strength becomes comparable to the vacuum term, i.e. at [18]

$$\frac{r_{\rm end}}{r_\nu} = \left(\frac{\mu_r\big|_{r=r_\nu}}{2\omega}\right)^{1/4} . \qquad (11)$$

We remind that outside $r_{\rm sync}$ the multi-angle nature of the neutrino trajectories in a supernova can lead to self-induced flavor decoherence between different angular modes. However, it has been shown in [43] that if the asymmetry parameter ϵ is significantly large, multi-angle effects are suppressed and self-induced neutrino oscillations exhibit a collective behavior. We will come back to this point in more details when commenting our numerical results.

Using the above definitions, in Fig. 4 we present the neutrinosphere radius r_ν, the synchronization radius $r_{\rm sync}$ and the radius $r_{\rm end}$ at which collective effects saturate, for the case of the 10.8 $M_\odot$ SN simulation. We see that $r_\nu \sim 10^2$ km during the accretion phase and drops to ~ 30 km at the beginning of the cooling phase. This contraction of the neutrinosphere radius reflects the gradual shift of the ν opacities. These change from being absorption dominated during the accretion, to being scattering dominated during the cooling [55, 56].

Collective oscillations are expected in the range $r \in [r_{\rm sync}, r_{\rm end}]$. This range is at $r \sim [600, 1500]$ km at $t_{\rm pb} = 0.1$ s when the neutrinosphere radius $r_\nu > 10^2$ km, pushing to larger radii the flavor conversions. Then, following the contraction of the neutrinosphere radius, the range of conversions shifts at smaller radii, moving to $r \sim [200, 500]$ km at $t_{\rm pb} \simeq 0.4$ s. Finally at $t_{\rm pb} \simeq 0.6$ s, the lower neutrino luminosity and the larger asymmetry parameter ϵ both conspire to push $r_{\rm sync}$ towards $r_{\rm end}$ [see Eqs. (10)–(11)].

In the range $[r_{\rm sync}, r_{\rm end}]$, the self-induced neutrino flavor conversions can be affected by the dense matter when [37]

$$n_e \gtrsim n_{\overline{\nu}_e} - n_{\overline{\nu}_x} . \qquad (12)$$

In particular, when the two densities are comparable matter effects induce multi-angle decoherence among different neutrino modes, leading to a flavor equilibration among the different species. When the net electron density is significantly larger than the neutrino density, collective oscillations are suppressed at all [37].

We remark that previous numerical studies of self-induced flavor conversions typically assumed smaller neutrinosphere radii, namely $r_\nu = \mathcal{O}(10$ km) (see, e.g., [43]). This choice is more appropriate for the cooling rather than for the accretion phase. As a consequence of this different input, in the current work flavor conversions start at larger radii than typically assumed in previous studies.

IV. MATTER EFFECTS FOR DIFFERENT PROGENITOR MASSES

In this Section we will present our results concerning the effects of dense matter on of the self-induced neutrino oscillations for the three representative SN simulations based on the different progenitor masses.

A. 10.8 $M_\odot$ progenitor mass

We start our investigation with the case of the 10.8 $M_\odot$ iron-core SN. In Fig. 5 we show the net electron density n_e (left panel) and the difference of neutrino densities $n_{\overline{\nu}_e} - n_{\overline{\nu}_x}$ (right panel) entering in the potential μ_r [Eq. (8)] for different post-bounce times. While the decline of the neutrino density is r^{-2}, the electron density presents a more complicated behavior. In particular, one can recognize the abrupt discontinuity in n_e associated with the supernova shock-front that propagates in time. The shock-wave initially dissipates its energy due to heavy nuclei dissociation and eventually stalls at $t_{\rm pb} = 0.05$ s. The standing accretion shock is revived via neutrino heating, on a timescale on the order of 0.1 seconds, and expands accordingly as well as contracts via neutrino cooling. After 0.35 seconds post-bounce, neutrino heating succeeds and the standing accretion shock turns into a dynamic shock with positive matter velocities. It initiates the onset of explosion at about 0.4 seconds post-bounce.

For this SN model we find that during the accretion phase the matter density in the post-shock region declines slower than the neutrino density, typically as $\sim r^{-1.5}$. From the comparison between the electron and

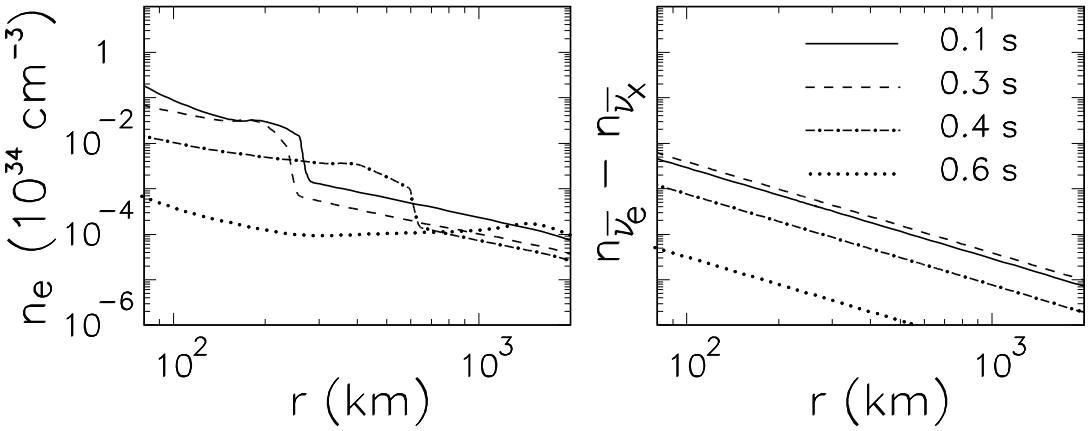


FIG. 5: 10.8 $M_\odot$ progenitor mass. Radial evolution of the net electron density n_e (left panel) and of the neutrino density difference $n_{\overline{\nu}_e} - n_{\overline{\nu}_x}$ (right panel) at different post-bounce times.

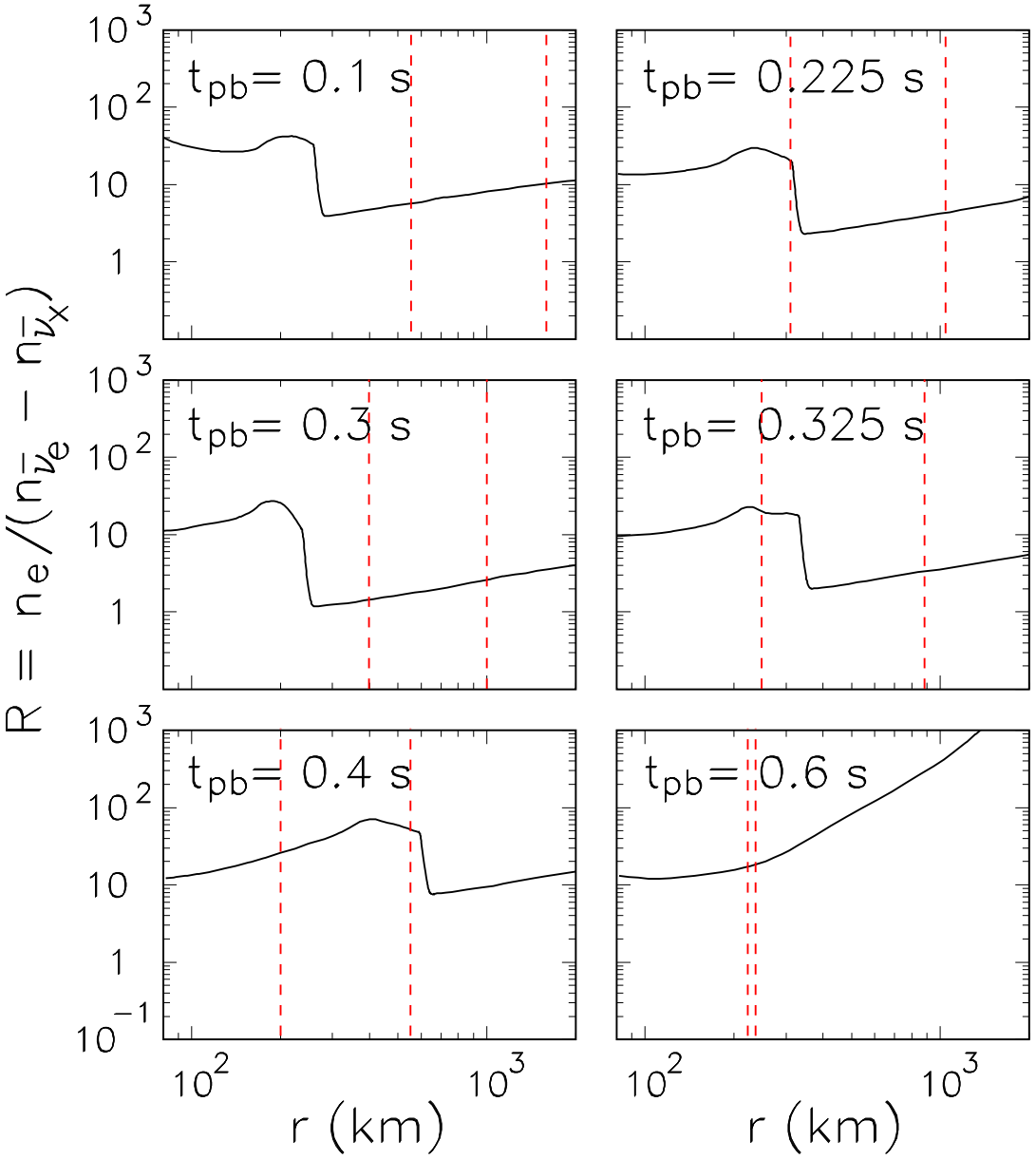


FIG. 6: 10.8 $M_\odot$ progenitor mass. Radial evolution of the ratio R between electron and neutrino densities at different post-bounce times. The two dashed vertical strips delimit the position of $r_{\rm sync}$ (left line) and $r_{\rm end}$ (right line).

the neutrino densities, we realize that at the different post-bounce times considered, n_e is always larger than or comparable to $n_{\overline{\nu}_e} - n_{\overline{\nu}_x}$. It suggests that one cannot ignore matter effects on self-induced flavor transformations during the accretion phase.

In order to quantify the relative strength of the electron and neutrino densities, in Fig. 6 we show the ratio

$$R = \frac{n_e}{n_{\overline{\nu}_e} - n_{\overline{\nu}_x}} \ . \tag{13}$$

as a function of the radial coordinate r at different post-bounce times for $t_{\rm pb} \in [0.1, 0.6]$ s. The range $r_{\rm sync} < r < r_{\rm end}$ is delimited with two vertical dashed lines. The values of $r_{\rm sync}$ and $r_{\rm end}$ determine the possible range for the self-induced flavor conversions and the shock radius $r_{\rm sh}$ denotes the abrupt drop in the electron density. Therefore, their relative position is crucial to assess the impact of matter effects. In the expected oscillation range, $R \gg 1$ will imply a strong matter dominance in the flavor conversions and thus complete suppression of the self-induced effects. Instead, when electron and neutrino densities are comparable ($R \gtrsim 1$), decoherence will occur for the collective oscillations.

The ratio R, being very large behind the shock front, prevents flavor conversions in this region. However, the ratio can go down to $R \gtrsim 1$ for $r > r_{\rm sh}$, leading to matter-induced decoherence and thus partial flavor changes.

Let us discuss in more detail what occurs at different post-bounce time snapshots in Fig. 6. At very early times ($t_{\rm pb} = 0.1$ s) the matter term is strongly dominant also behind the shock-front ($R \gg 1$). Under these conditions oscillations are always blocked. Then, at intermediate times ($t_{\rm pb} = 0.225, 0.3$ s) the matter density in the post-shock region, where flavor conversions are possible, is dropping faster than the neutrino one. Therefore, the ratio R drops at 1-2 in this range and matter-induced decoherence is possible in this case. Subsequently, at $t_{\rm pb} = 0.325$ s, oscillations are suppressed behind the shock front, but then decoherence will develop at larger radii ($r \gtrsim 300$ km) when $R \gtrsim 1$. Eventually at later times ($t_{\rm pb} = 0.4, 0.6$ s), since the shock has resumed its forward motion, the region relevant for the oscillations is at $r < r_{\rm sh}$, where $R \gg 1$. In this situation self-induced oscillations will be suppressed. From these different snapshots we realize that R has a peculiar non-monotonic behavior as a function of time. It suggests a time-dependent pattern for the matter effects on the self-induced transitions during the accretion phase, namely complete–partial–complete suppression.

In order to confirm these expectations, we have performed a multi-angle numerical study of the equations for the neutrino flavor evolution in the schematic model described in Section III. Our treatment closely follows the one presented in Ref. [37] to which we address the interested reader for further details. We only mention here that in order to achieve convergence in our simulations we had to simulate 10^3 neutrino angular modes. In Fig. 7 we show the radial evolution of the $\overline{\nu}_e$ survival probability P_{ee} for different post-bounce times, obtained taking into account the effects of the SN matter profile (continuous curve). For comparison, we show also the results obtained setting $n_e = 0$ (dashed curve).

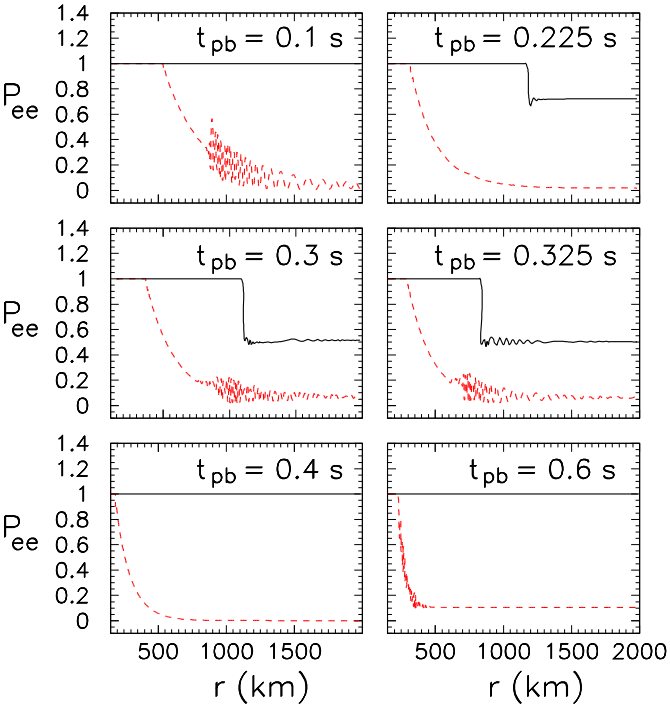


FIG. 7: 10.8 $M_\odot$ progenitor mass. Radial evolution of the survival probability P_{ee} for electron antineutrinos at different post-bounce times for the multi-angle evolution in presence of matter effects (continuous curve) and for $n_e = 0$ (dashed curve).

In the case with $n_e = 0$, for the given flavor asymmetry $\epsilon \gtrsim 0.3$ we would have expected the "quasi-single angle" behavior described in Ref. [43], where after the onset of the conversions at $r = r_{\rm sync}$, the survival probability P_{ee} declines smoothly approaching zero at large radii. However, in the situation we are studying flavor conversions develop at radii larger than what is typically shown in previous works (see, e.g., [43]). Therefore, the evolution is more adiabatic (i.e. the evolution length scale $l_\mu \sim r$ [30]). As a consequence, effects of self-induced multi-angle decoherence have more chances to develop in this case, producing some small disturbance in the smooth decline of the survival probability at large radii (visible at $t_{\rm pb} = 0.1, 0.3, 0.325$ s for $r \gtrsim 700$ km). This finding is potentially interesting, however, since matter effects will anyhow dramatically alter this picture we have not performed a systematic study on this (sub-leading) self-induced decoherence.

Passing now to the matter case, we see that at $t_{\rm pb} = 0.1, 0.4, 0.6$ s the flavor oscillations are completely blocked, since $R \gg 1$ in the conversion range. For the other three intermediate times ($t_{\rm pb} = 0.225, 0.3, 0.325$ s), the presence of a large matter term at $r_{\rm sync}$ will significantly delay the onset of the flavor conversions with re-

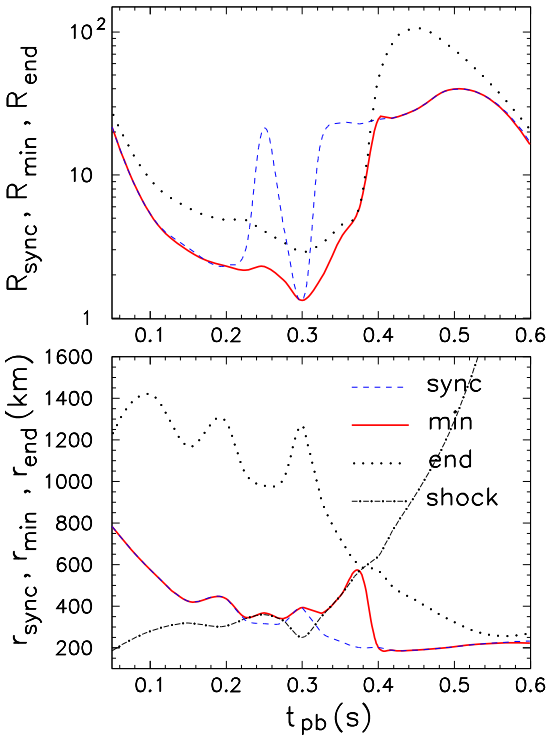


FIG. 8: 10.8 $M_\odot$ progenitor mass. Upper panel: Time evolution of the ratio $R_{\rm sync}$ (dashed curve), $R_{\rm min}$ (continuous curve) and $R_{\rm end}$ (dotted curve). Lower panel: Time evolution of the radial position $r_{\rm sync}$ (dashed curve), $r_{\rm min}$ (continuous curve), $r_{\rm end}$ (dotted curve) and $r_{\rm shock}$ (dot-dashed curve).

spect to the case with $n_e = 0$. Then, at larger radii ($r > 700$ km) when $R \gtrsim 1$–2, matter effects produce a partial suppression of the flavor conversions, with a tendency toward flavor decoherence. When the latter is complete, it leads to $P_{ee} \to 1/2$ (at $t_{\rm pb} = 0.3, 0.325$ s), implying a complete mixture between $\overline{\nu}_e$ and $\overline{\nu}_x$.

Finally, we would summarize our results with a figure of merit that captures in a compact way the interplay between matter and self-induced effects as a function of time. Therefore, in Fig. 8 we show the ratio R (upper panel) at its minimum value

$$R_{\rm min} = \min \left(\frac{n_e}{n_{\overline{\nu}_e} - n_{\overline{\nu}_x}} \right)_{r \in [r_{\rm sync}; r_{\rm end}]} , \qquad (14)$$

in the range $r \in [r_{\rm sync}; r_{\rm end}]$ relevant for collective conversions. This value provides a conservative estimation for the impact of matter effects. Indeed, if $R_{\rm min} \gg 1$ one should expect a complete matter suppression of the flavor changes. Conversely, when $R_{\rm min} \gtrsim 1$ the matter suppression will be partial and will lead to flavor decoherence. For comparison we also show the values of R at the two radii $r_{\rm sync}$ and $r_{\rm end}$. Moreover, in the lower panel we represent the time evolution of the radial positions $r_{\rm sync}$, $r_{\rm end}$, $r_{\rm min}$ and $r_{\rm sh}$.

One realizes that R presents a non-trivial behavior in the range between $r_{\rm sync}$ and $r_{\rm end}$. In particular, the position of the minimum value $R_{\rm min}$ is at

$$r_{\rm min} = \begin{cases} r_{\rm sh} & \text{if} \quad r_{\rm sync} < r_{\rm sh} < r_{\rm end} \\ r_{\rm sync} & \text{otherwise} \end{cases} \qquad (15)$$

For $t_{\rm pb} \lesssim 0.3$ s, since the neutrino density grows and the electron density decreases in time, $R_{\rm min}$ decreases monotonically from $\sim$20 at $t_{\rm pb} = 0.05$ s to $\sim$1–2 at $t_{\rm pb} \simeq 0.3$ s post-bounce, changing from complete to partial matter suppression. Then, since at the end of the accretion phase the neutrino density decreases faster than the electron density, $R_{\rm min}$ rises again to $\sim$20 at $t_{\rm pb} \simeq 0.4$–0.6 s, suppressing flavor conversions. The behavior of $R_{\rm min}$ shows in a compact way the succession of phases with complete–partial–complete matter suppression in the time evolution of the neutrino self-induced conversions during the accretion phase.

A similar analysis to the one presented above based on Fig. 8, may allow to obtain a first answer about the role of the matter on the self-induced effects. This schematic approach does not require a detailed numerical study of the neutrino flavor evolution. For this reason, we find it useful to compare the role of matter in different SN simulations based on different progenitor models. In the following, we will apply such analysis to the other SN simulations from Ref. [7] based on different progenitor masses.

B. 18.0 $M_\odot$ progenitor mass

As further example, we consider the SN simulation of the more massive 18 $M_\odot$ iron-core progenitor. In Fig. 9 we show the net electron density n_e (left panel) and the difference of neutrino densities $n_{\overline{\nu}_e} - n_{\overline{\nu}_x}$ for different post-bounce times. From the comparison with Fig. 5 we see that the time evolution of the electron and neutrino density profiles is similar to the case 10.8 $M_\odot$ SN simulation. Therefore, we expect a similar impact for the matter effects on the neutrino flavor evolution. In Fig. 10 we show the time evolution of $R_{\rm min}$ in the same format as in Fig. 8. We see that the behavior of $R_{\rm min}$ is also very similar to the previous case described above. Therefore, one expect an analogous pattern of complete ($0.05 \lesssim t_{\rm pb} \lesssim 0.2$ s), partial ($0.2 \lesssim t_{\rm pb} \lesssim 0.35$ s) and complete ($0.35 \lesssim t_{\rm pb} \lesssim 0.6$ s) matter suppression in the self-induced flavor conversions.

We have repeated the same analysis also for a 15.0 $M_\odot$ iron-core progenitor mass, giving a not-exploding supernova. In the time range before the recollapse of the star ($t_{\rm pb} \lesssim 0.3$ s) the results obtained are similar to the one shown for the two exploding cases. Therefore, for the sake of the brevity, we will not show them here.

C. 8.8 $M_\odot$ progenitor mass

Finally, we pass to analyze the case of the SN of the low mass 8.8 $M_\odot$ O-Ne-Mg core. In Fig. 11 we present

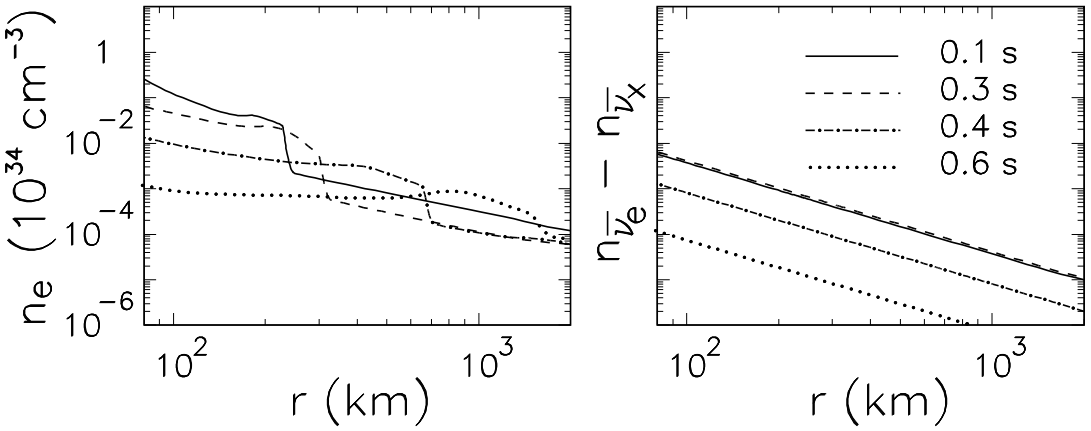


FIG. 9: 18.0 $M_\odot$ progenitor mass. Radial evolution of the net electron density n_e (left panel) and of the neutrino density difference $n_{\overline{\nu}_e} - n_{\overline{\nu}_x}$ (right panel) at different post-bounce times.

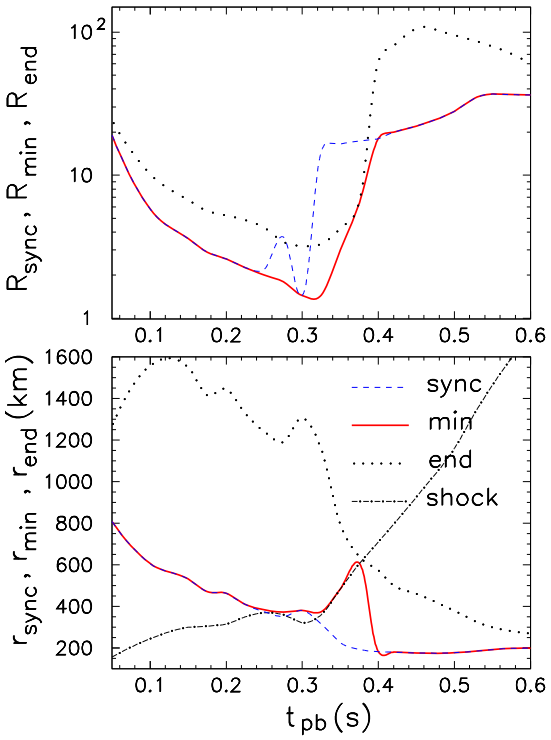


FIG. 10: 18.0 $M_\odot$ progenitor mass. Upper panel: Time evolution of the ratio $R_{\rm sync}$ (dashed curve), $R_{\rm min}$ (continuous curve) and $R_{\rm end}$ (dotted curve). Lower panel: Time evolution of the radial position $r_{\rm sync}$ (dashed curve), $r_{\rm min}$ (continuous curve), $r_{\rm end}$ (dotted curve) and $r_{\rm shock}$ (dash-dotted curve).

the net electron density n_e (left panel) and the difference of neutrino densities $n_{\overline{\nu}_e} - n_{\overline{\nu}_x}$ (right panel) for different post-bounce times. We realize that since in this case the matter density of the envelope is very low compared to the iron-core progenitors, the electron density profile above the core is very steep, declining as $\sim r^{-2.5}$, faster than the neutrino density. Moreover, also the neutrino densities for $t_{\rm pb} \lesssim 0.2$ s are roughly a factor ~ 3 smaller than in the case of the iron-core supernovae. This reflects the practical absence of an extended accretion phase for this low-mass star. In this case the explosion succeeds very shortly after the core-bounce. Therefore, the shock-front is already beyond the radial range interesting for the flavor conversions.

Fig. 12 shows the time evolution of $R_{\rm min}$ in the range $r \in [r_{\rm sync}; r_{\rm end}]$ relevant for collective conversions. We realize that the behavior of $R_{\rm min}$ is different with respect to the previously considered iron-core supernovae. Since in this case the matter does not present an abrupt discontinuity, but it monotonically decreases, the position of $R_{\rm min}$ will always coincide with $r_{\rm end}$. Moreover, since the electron density is never much larger than the neutrino density in the conversion region, it results in $R_{\rm min} \lesssim 3$.

The peculiar time evolution of $R_{\rm min}$ in this case will depend on the small differences between the matter and the neutrino term. At $t_{\rm pb} \lesssim 0.13$ s, the electron density is smaller than the neutrino density in the range of collective conversions, giving $R_{\rm min} \lesssim 1$. Then, the ratio $R_{\rm min}$ grows up to $\sim 2-3$ at $t_{\rm pb} \simeq 0.2$ s since the electron density in the conversion region is larger than in the previous case. As a result, the time-evolution of the neutrino survival probabilities presents a change between a regime dominated by the ν–ν effects at very early times and one of matter-suppressed oscillations at later times.

In Fig. 13 we explicitly show this behavior, representing the radial evolution of the $\overline{\nu}_e$ survival probability P_{ee} for the same post-bounce times snapshots of Fig. 11, with (continuous curves) and without (dashed curves) matter. We find that at $t_{\rm pb} = 0.08$ s where $R \lesssim 1$, the matter suppression is relatively small and the neutrino-neutrino interactions produce a quite almost complete swap between $\overline{\nu}_e$ and $\overline{\nu}_x$ spectra ($P_{ee} = 0.15$ at the end of the evolution). Conversely, for the later times considered, the flavor conversions are strongly suppressed with a final $P_{ee} \simeq 0.7-0.9$, since $R \gtrsim 1$. We want to remark that the time evolution of the neutrino oscillation probability during the accretion phase is significantly different with

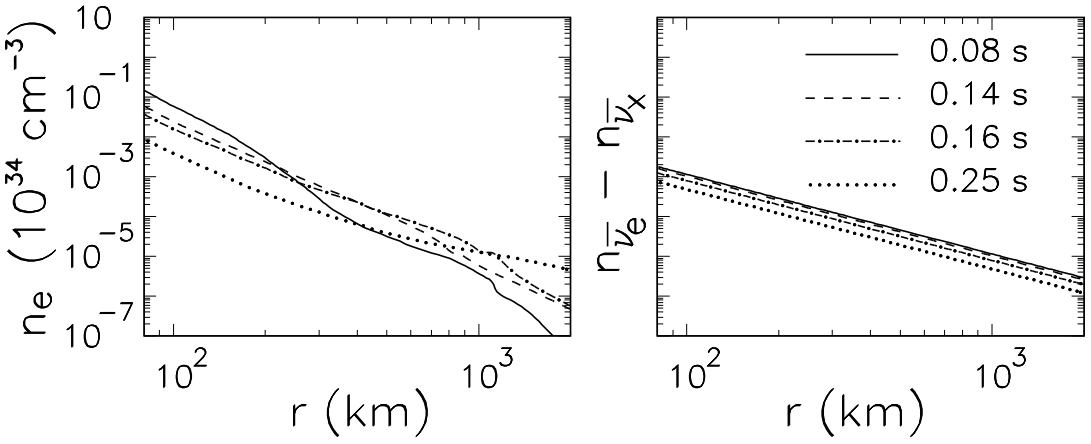


FIG. 11: 8.8 $M_\odot$ progenitor mass. Radial evolution of the net electron density n_e (left panel) and of the neutrino density difference $n_{\overline{\nu}_e} - n_{\overline{\nu}_x}$ (right panel) at different post-bounce times.

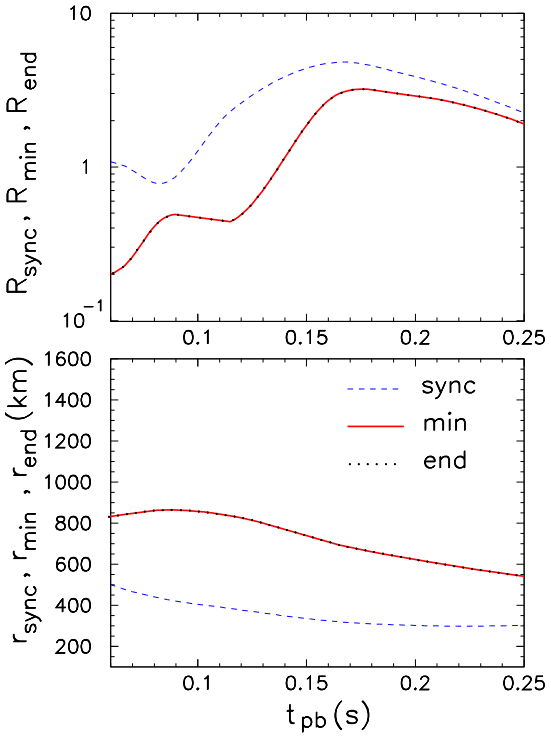


FIG. 12: 8.8 $M_\odot$ progenitor mass. Upper panel: Time evolution of the ratio $R_{\rm sync}$ (dashed curve), $R_{\rm min}$ (continuous curve) and $R_{\rm end}$ (dotted curve). Lower panel: Time evolution of the radial position $r_{\rm sync}$ (dashed curve), $r_{\rm min}$ (continuous curve), $r_{\rm end}$ (dotted curve).

respect to the case of the iron-core supernovae we studied. This will allow the distinction of a O-Ne-Mg-core SN from a iron-core SN, in the case of the detection of a future galactic event.

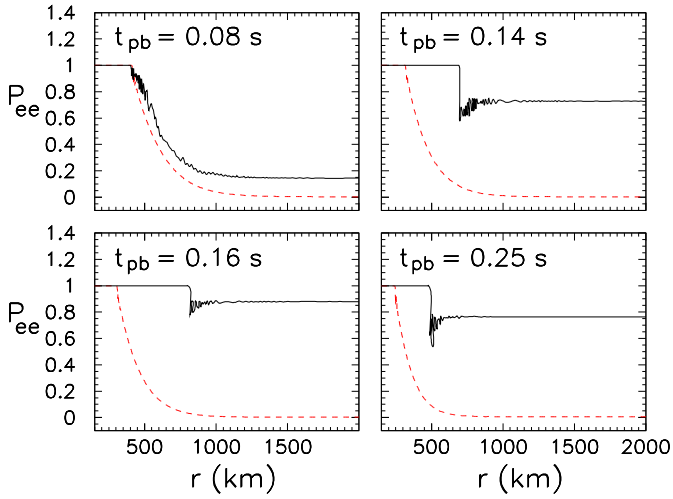


FIG. 13: 8.8 $M_\odot$ progenitor mass. Radial evolution of the survival probability P_{ee} for electron antineutrinos at different post-bounce times for the multi-angle simulations in presence of matter effects (continuous curve) and for the case with $n_e = 0$ (dash-dotted curve).

V. EARTH MATTER EFFECT DURING THE ACCRETION PHASE

It is plausible that a high-statistics neutrino detection from a future galactic SN [57, 58] would faithfully monitor the abrupt time variations imprinted on the neutrino oscillation probabilities by the transitions between stages of complete and partial matter suppression during the accretion phase. We plan to perform a dedicated investigation of the matter suppression during the accretion phase on the observable SN neutrino burst in a future work.

Here we discuss another consequence of the SN dense matter effects, namely the change of the interpretation of the Earth matter effect on the supernova neutrino sig-

nal. It is widely known that if SN neutrinos arrive at the detector from "below", the Earth crossing will induce an energy-dependent modulation in the neutrino survival probability [59]. The appearance of the Earth effect depends on the neutrino fluxes and on the mixing scenario. The accretion phase is particularly promising to detect Earth crossing signatures because the absolute SN ν flux is large and the flavor-dependent flux differences are also large.

Before the inclusion of the collective effects in the SN neutrino flavor transitions, the detection of Earth matter modulations has been proposed as a tool to distinguish the neutrino mass hierarchy at "large" values of the mixing angle θ_{13} (i.e. $\sin^2\theta_{13} \gtrsim 10^{-3}$) [60]. Then, when collective oscillations were taken into account, it was speculated that due to the self-induced flavor transformations, the presence or absence of Earth matter effects will break the degeneracy between normal and inverted mass hierarchy for "small" values of the mixing angle θ_{13} (i.e. $\sin^2\theta_{13} \lesssim 10^{-5}$) while no hierarchy discrimination is possible for larger values of θ_{13} [61]. Now, due to the matter suppression effect this conclusion should be revisited for the accretion phase.

To determine the observable SN neutrino fluxes at Earth, we refer to [54]. We consider the modified flavor basis, (ν_e, ν_x, ν_y), which is defined such that $(\nu_e, \nu_x, \nu_y) = {R_{23}}^{\dagger}(\theta_{23})(\nu_e, \nu_\mu, \nu_\tau)$, where R_{23} is the 2–3 rotation matrix. This will allow for collective oscillations between e and y states. For definiteness, here we concentrate on the $\overline{\nu}_e$ spectra observable through inverse beta decay reactions, $\overline{\nu}_e + p \longrightarrow n + e^+$, at water/ice Cherenkov or scintillation detectors [57, 62].

In normal hierarchy, the $\overline{\nu}_e$ flux at Earth, $F^D_{\overline{\nu}_e}$, (without collective effect and no MSW effect associated to θ_{13}) for any value of the mixing angle θ_{13} is given by [60]

$$F^D_{\bar{\nu}_e} = \cos^2\theta_{12} F_{\bar{\nu}_e} + \sin^2\theta_{12} F_{\bar{\nu}_x} \ , \qquad (16)$$

where θ_{12} is the 1–2 mixing angle, with $\sin^2\theta_{12} \simeq 0.3$ [52, 53].

In the inverted mass hierarchy, MSW matter effects in the SN envelope are characterized in terms of the level-crossing probability P_H of antineutrinos, which is in general a function of the neutrino energy and θ_{13} [36]. In the following, we consider two extreme limits, namely $P_H \to 0$ when $\sin^2\theta_{13} \gtrsim 10^{-3}$ ("large"), and $P_H \to 1$ when $\sin^2\theta_{13} \lesssim 10^{-5}$ ("small"). In this situation and for complete matter suppression of collective oscillations for large θ_{13} , $F^D_{\bar{\nu}_e}$ is given by

$$F^D_{\bar{\nu}_e} = F_{\bar{\nu}_x} \ , \qquad (17)$$

while small θ_{13} results in the same case as for normal hierarchy [Eq. (16)].

In the case of matter-induced docoherence between $\overline{\nu}_e$ and $\overline{\nu}_y$ in inverted hierarchy, leading to a complete mixture of $\overline{\nu}_e$ and $\overline{\nu}_y$, the detectable $\overline{\nu}_e$ flux for any value of the mixing angle θ_{13} would be given by

$$F^D_{\bar{\nu}_e} = \cos^2\theta_{12} \frac{F_{\bar{\nu}_e} + F_{\bar{\nu}_y}}{2} + \sin^2\theta_{12} F_{\bar{\nu}_x} \ . \qquad (18)$$

Earth effect can be taken into account by just mapping $\cos^2\theta_{12} \to P(\overline{\nu}_1 \to \overline{\nu}_e)$ and $\sin^2\theta_{12} \to 1 - P(\overline{\nu}_1 \to \overline{\nu}_e)$. where $P(\overline{\nu}_1 \to \overline{\nu}_e)$ is the probability that a state entering the Earth as mass eigenstate $\overline{\nu}_1$ is detected as $\overline{\nu}_e$ at the detector [59].

Considering for definiteness the case of iron-core SNe, the presence or absence of Earth matter effects at early times ($t_{\rm pb} \lesssim 0.2$ s) will allow to distinguish the neutrino mass hierarchy at large value of the mixing angle θ_{13} [see Eqs. (16)–(17)]. Moreover, the Earth effects may become observable via the interesting time pattern introduced above, in the case of inverted mass hierarchy at large θ_{13}: *(1)* no effects at early times [Eq. (17)], *(2)* the appearance at intermediate times when decoherence occurs [Eq. (18)], and *(3)* disappearance again when the accretion rate decreases significantly.

VI. DISCUSSION AND CONCLUSIONS

Different simulations of core-collapse SNe [39–42], show independently that the matter density in the stellar interior is large during the post-bounce accretion phase before the onset of an explosion. This implies that self-induced neutrino flavor transformations are affected by the high matter density, through trajectory-dependent phenomena [37].

In order to characterize the SN ν flavor evolution quantitatively, we performed a dedicated study, where we took as benchmark for the SN neutrino emissivity and the matter profiles the recent long-term core-collapse SN simulations from Ref. [7]. We considered three different cases for the supernova progenitor mass, the low mass 8.8 $M_\odot$ O-Ne-Mg-core and the two more massive iron-core progenitors of 10.8 and 18 $M_\odot$. In all three cases the electron density n_e is never negligible in comparison to the neutrino density n_ν during the accretion phase. As a consequence, the trajectory-dependent matter effects always influence the development of the self-induced transformations. We realized that during the accretion phase both the condition of matter suppression ($n_e \gg n_\nu$) and matter-induced decoherence ($n_\nu \sim n_e$) are realized. This implies that interesting time-dependent features in the neutrino signal can occur at early times. Moreover, the different patterns of complete/partial matter suppression would allow, at least in principle, to distinguish from the flavor evolution between iron-core and O-Ne-Mg core SNe.

In early schematic investigations, the accretion phase seemed a particularly clear setup to probe the development of the collective neutrino transformations, because the expected flux hierarchy is large and robust. In such a situation the pattern of the self-induced spectral swaps/splits were thought to be unambiguous [32]. In this scenario, the presence or absence of Earth matter effects on the SN neutrino burst were proposed to break the degeneracy between normal and inverted mass hierarchy for "small" values of the mixing angle θ_{13} [61].

Our findings seem to change this picture once more. In particular, the dense matter suppression of collective oscillations in supernovae implies that Earth matter effects may allow to distinguish the neutrino mass hierarchy in the likely case of large θ_{13} [63], as originally expected in the analysis performed without the inclusion of the collective phenomena. This intriguing possibility makes supernova neutrino detection a competitive way to get this yet unknown property of the neutrino mass spectrum in addition to terrestrial experiments [64].

Furthermore, in the past [16, 39] it has been speculated that swaps of neutrino fluxes between electron and non-electron flavors in the deepest SN regions may increase the neutrino energy deposition and hence the neutrino heating in the gain region behind the standing bounce shock. It was argued that it could possibly help to revive the shock and to trigger neutrino-driven explosions. We have shown that the presence of the matter suppression of flavor conversions at high densities, behind the shock front (see, e.g., Fig. 6), implies that these cannot play any significant role in changing the neutrino energy deposition rate behind the stalled shock-wave. As an important consequence, the problem of he ν flavor mixing in SNe can be decoupled from the ν transport and impact on the matter heating/cooling. This result is confirmed by the analysis recently performed in [65] using two-dimensional supernova models. In that work, even if multi-angle matter effects are not included in the simulation of the flavor oscillations, a negligible impact of the self-induced conversions is found on the energy deposition behind the shock-wave. Indeed, we also find that neglecting matter effects, the possible range where self-induced oscillations would have significantly developed is always after the shock-wave position ($r_{\rm sh} \lesssim r_{\rm sync}$) at the times relevant for the shock revival (see our Fig. 6–8).

Our results have been obtained considering a spherically symmetric neutrino emission. All the previous analysis in the field have relied on this assumption to make the flavor evolution equations numerically tractable. It remains to be investigated if the removal of a perfect spherical symmetry can provide a different behavior in the flavor evolution [66]. Moreover, in multi-dimensional SN models density fluctuations are expected behind the standing bounce shock, due to the presence of convection and hydro instabilities. These can range at most between 10% to a factor 2-3 (see, e.g., [40, 67]). Therefore, even in the case a fraction of neutrinos beam crosses underdenses regions, the matter suppression of the collective oscillations will still remain relevant. This claim is supported by a recent analysis of the matter suppression, performed with two-dimensional SN simulations [65].

Self-induced effects in the supernova neutrinos still remain crucial during the later cooling phase, when the matter density decreases continuously ($t_{\rm pb} \gtrsim 1$ s) and becoming sub-dominant with respect to the neutrino density. In this situation and for the flux ordering provided by the simulations from Ref. [7], we confirm that self-induced oscillations in the cooling phase produce multiple splits and swaps, like the one described in [26–32]. Moreover, for low-mass O-Ne-Mg-core SN a peculiar interplay of MSW and self-induced effects would produce interesting signatures during the ν_e prompt neutronization burst [68–70].

In conclusion, the time evolution of the SN neutrino signal provides a large amount of information on the flavor transformations of neutrinos in the deepest stellar regions. The early post-bounce deleptonization, accretion and cooling phases represent three different "experiments" that allow us to probe different behaviors of the dense SN neutrino gas. In order to learn the most from a future neutrino observation from a galactic event, improved theoretical and experimental studies are necessary to decipher the supernova neutrino enigma.

Acknowledgments

We thank B. Dasgupta, T. Janka, G. Raffelt, C. Ott and G. Sigl for useful discussions and suggestions during the development of this project. We also acknowledge E. Lisi, G. Raffelt, S. Sarikas, and I. Tamborra for helpful comments on the manuscript. The work of S.C., A.M., N.S. was supported by the German Science Foundation (DFG) within the Collaborative Research Center 676 "Particles, Strings and the Early Universe". T.F. acknowledges support from HIC for FAIR project no. 62800075.

References

[1] J. M. LeBlanc and J. R. Wilson, "A Numerical Example of the Collapse of a Rotating Magnetized Star" Astrophys. J., **161**, 541 (1970).

[2] A. Burrows, E. Livne, L. Dessart, C. D. Ott and J. Murphy, "Features of the Acoustic Mechanism of Core-Collapse Supernova Explosions" Astrophys. J., **655**, 416 (2006).

[3] H. Bethe and J. R. Wilson "Revival of a stalled supernova shock by neutrino heating" Astrophys. J. **295**, 14 (1985).

[4] F. S. Kitaura, H.-Th. Janka and W. Hillebrandt, "Explosions of O-Ne-Mg cores, the crab supernova, and subluminous type II-p supernovae " Astron. Astrophys. **450**, 345 (2006).

[5] I. Sagert, T. Fischer, M. Hempel, G. Pagliara, J.Schaffner-Bielich, J. A. Mezzacappa, F.-K. Thielemann and M. Liebendörfer, "Signals of the QCD phase transition in core-collapse supernovae" Phys. Rev. Lett. **102**, 081101 (2009).

[6] T. Fischer, I. Sagert, G. Pagliara, M. Hempel, J. Schaffner-Bielich, T. Rauscher, F.-K. Thielemann, R. Käppeli, G. Martínez-Pinedo and M. Liebendörfer, "Core collapse supernova explosions triggered by a quark-hadron phase transition during the early post-bounce phase" Astrophy. J. (in press).

[7] T. Fischer, S. C. Whitehouse, A. Mezzacappa, F. K. Thielemann and M. Liebendorfer, "Protoneutron star evolution and the neutrino driven wind in general relativistic neutrino radiation hydrodynamics simulations," Astron. Astrophys. **517**, A80 (2010). [arXiv:0908.1871 [astro-ph.HE]].

[8] B. Dasgupta, "Physics and Astrophysics Opportunities with Supernova Neutrinos," arXiv:1005.2681 [hep-ph].

[9] L. Wolfenstein, "Neutrino Oscillations In Matter," Phys. Rev. D **17**, 2369 (1978); S. P. Mikheev and A. Yu. Smirnov, "Resonance Enhancement Of Oscillations In Matter And Solar Neutrino Spectroscopy," Yad. Fiz. **42**, 1441 (1985) [Sov. J. Nucl. Phys. **42**, 913 (1985)].

[10] J. T. Pantaleone, "Neutrino Flavor Evolution Near A Supernova's Core," Phys. Lett. B **342**, 250 (1995) [astro-ph/9405008].

[11] Y. Z. Qian, G. M. Fuller, G. J. Mathews, R. Mayle, J. R. Wilson and S. E. Woosley, "A Connection Between Flavor Mixing Of Cosmologically Significant Neutrinos And Heavy Element Nucleosynthesis In Supernovae," Phys. Rev. Lett. **71**, 1965 (1993).

[12] Y. Z. Qian and G. M. Fuller, "Neutrino-neutrino scattering and matter enhanced neutrino flavor transformation in Supernovae," Phys. Rev. D **51**, 1479 (1995) [astro-ph/9406073].

[13] S. Pastor and G. Raffelt, "Flavor oscillations in the supernova hot bubble region: Nonlinear effects of neutrino background," Phys. Rev. Lett. **89**, 191101 (2002) [astro-ph/0207281].

[14] G. M. Fuller and Y. Z. Qian, "Simultaneous Flavor Transformation of Neutrinos and Antineutrinos with Dominant Potentials from Neutrino-Neutrino Forward Scattering," Phys. Rev. D **73**, 023004 (2006) [astro-ph/0505240].

[15] H. Duan, G. M. Fuller and Y. Z. Qian, "Collective Neutrino Flavor Transformation In Supernovae," Phys. Rev. D **74**, 123004 (2006) [astro-ph/0511275].

[16] H. Duan, G. M. Fuller, J. Carlson and Y. Z. Qian, "Simulation of coherent non-linear neutrino flavor transformation in the supernova environment. I: Correlated neutrino trajectories," Phys. Rev. D **74**, 105014 (2006) [astro-ph/0606616].

[17] H. Duan, G. M. Fuller and Y. Z. Qian, "Collective Neutrino Oscillations," Ann. Rev. Nucl. Part. Sci. **60**, 569 (2010) [arXiv:1001.2799 [hep-ph]].

[18] G. L. Fogli, E. Lisi, A. Marrone and A. Mirizzi, "Collective neutrino flavor transitions in supernovae and the role of trajectory averaging," JCAP **0712**, 010 (2007) [arXiv:0707.1998 [hep-ph]].

[19] G. L. Fogli, E. Lisi, A. Marrone, A. Mirizzi and I. Tamborra, "Low-energy spectral features of supernova (anti)neutrinos in inverted hierarchy," Phys. Rev. D **78**, 097301 (2008) [arXiv:0808.0807 [hep-ph]].

[20] G. G. Raffelt and A. Y. Smirnov, "Self-induced spectral splits in supernova neutrino fluxes," Phys. Rev. D **76**, 081301 (2007) [Erratum-ibid. D **77**, 029903 (2008)] [arXiv:0705.1830 [hep-ph]].

[21] G. G. Raffelt, A. Y. Smirnov, "Adiabaticity and spectral splits in collective neutrino transformations," Phys. Rev. **D76**, 125008 (2007). [arXiv:0709.4641 [hep-ph]].

[22] H. Duan, G. M. Fuller, J. Carlson *et al.*, "Neutrino Mass Hierarchy and Stepwise Spectral Swapping of Supernova Neutrino Flavors," Phys. Rev. Lett. **99**, 241802 (2007). [arXiv:0707.0290 [astro-ph]].

[23] H. Duan, G. M. Fuller, Y. -Z. Qian, "Stepwise spectral swapping with three neutrino flavors," Phys. Rev. **D77**, 085016 (2008). [arXiv:0801.1363 [hep-ph]].

[24] J. Gava and C. Volpe, "Collective neutrinos oscillation in matter and CP-violation," Phys. Rev. D **78**, 083007 (2008) [arXiv:0807.3418 [astro-ph]].

[25] J. Gava, J. Kneller, C. Volpe and G. C. McLaughlin, "A dynamical collective calculation of supernova neutrino signals," Phys. Rev. Lett. **103**, 071101 (2009) [arXiv:0902.0317 [hep-ph]].

[26] B. Dasgupta, A. Dighe, G. G. Raffelt and A. Y. Smirnov, "Multiple Spectral Splits of Supernova Neutrinos," Phys. Rev. Lett. **103**, 051105 (2009) [arXiv:0904.3542 [hep-ph]].

[27] G. Fogli, E. Lisi, A. Marrone and I. Tamborra, "Supernova neutrinos and antineutrinos: ternary luminosity diagram and spectral split patterns," JCAP **0910** (2009) 002 [arXiv:0907.5115 [hep-ph]].

[28] S. Chakraborty, S. Choubey, S. Goswami and K. Kar, "Collective Flavor Oscillations Of Supernova Neutrinos and r-Process Nucleosynthesis," JCAP **1006**, 007 (2010) [arXiv:0911.1218 [hep-ph]].

[29] A. Friedland, "Self-refraction of supernova neutrinos: mixed spectra and three-flavor instabilities," Phys. Rev. Lett. **104**, 191102 (2010) [arXiv:1001.0996 [hep-ph]].

[30] B. Dasgupta, A. Mirizzi, I. Tamborra and R. Tomàs, "Neutrino mass hierarchy and three-flavor spectral splits of supernova neutrinos," Phys. Rev. D **81**, 093008 (2010) [arXiv:1002.2943 [hep-ph]].

[31] H. Duan and A. Friedland, "Self-induced suppression of collective neutrino oscillations in a supernova," Phys. Rev. Lett. **106**, 091101 (2011) [arXiv:1006.2359 [hep-ph]].

[32] A. Mirizzi and R. Tomas, "Multi-angle effects in self-induced oscillations for different supernova neutrino fluxes," arXiv:1012.1339 [hep-ph].

[33] S. Galais, J. Kneller and C. Volpe, "The neutrino-neutrino interaction effects in supernovae: the point of view from the matter basis," arXiv:1102.1471 [astro-ph.SR].

[34] S. Galais and C. Volpe, "The neutrino spectral split in core-collapse supernovae: a magnetic resonance phenomenon," arXiv:1103.5302 [astro-ph.SR].

[35] S. Hannestad, G. G. Raffelt, G. Sigl and Y. Y. Y. Wong, "Self-induced conversion in dense neutrino gases: Pendulum in flavour space," Phys. Rev. D **74**, 105010 (2006) [Erratum-ibid. D **76**, 029901 (2007)] [astro-ph/0608695].

[36] A. S. Dighe and A. Y. Smirnov, "Identifying the neutrino mass spectrum from the neutrino burst from a supernova," Phys. Rev. D **62**, 033007 (2000) [hep-ph/9907423].

[37] A. Esteban-Pretel, A. Mirizzi, S. Pastor, R. Tomas, G. G. Raffelt, P. D. Serpico and G. Sigl, "Role of dense matter in collective supernova neutrino transformations," Phys. Rev. D **78**, 085012 (2008) [arXiv:0807.0659 [astro-ph]].

[38] H. Duan, G. M. Fuller and Y. Z. Qian, "Symmetries in collective neutrino oscillations," J. Phys. G **36**, 105003 (2009) [arXiv:0808.2046 [astro-ph]].

[39] G. M. Fuller, R. Mayle, B. S. Meyer and J. R. Wilson, "Can a closure mass neutrino help solve the supernova shock reheating problem ?," Astrophys. J. **389**, 517 (1992).

[40] R. Tomas, M. Kachelriess, G. Raffelt, A. Dighe, H. T. Janka and L. Scheck, "Neutrino signatures of supernova shock and reverse shock propagation," JCAP **0409**, 015 (2004) [astro-ph/0407132].

[41] R. Buras, M. Rampp, H. T. Janka and K. Kifonidis, "Two-dimensional hydrodynamic core-collapse supernova simulations with spectral neutrino transport. I. Numerical method and results for a 15 $M_{\rm sun}$ star," Astron. Astrophys. **447**, 1049 (2006) [astro-ph/0507135].

[42] M. Liebendoerfer, M. Rampp, H. T. Janka and A. Mezzacappa, "Supernova Simulations with Boltzmann Neutrino Transport: A Comparison of Methods," Astrophys. J. **620**, 840 (2005) [astro-ph/0310662].

[43] A. Esteban-Pretel, S. Pastor, R. Tomàs, G. G. Raffelt and G. Sigl, "Decoherence in supernova neutrino transformations suppressed by deleptonization," Phys. Rev. D **76**, 125018 (2007) [arXiv:0706.2498 [astro-ph]].

[44] S. Chakraborty, T. Fischer, A. Mirizzi, N. Saviano and R. Tomas, "No collective neutrino flavor conversions during the supernova accretion phase," arXiv:1104.4031 [hep-ph].

[45] K. Nomoto, "Evolution of 8–10 $M_\odot$ stars toward electron capture supernovae. I. Formation of electron-degenerate O + Ne + Mg cores," Astrophys. J. **277**, 791 (1984).

[46] K. Nomoto, "Evolution of 8–10 $M_\odot$ stars toward electron capture supernovae. II. Collapse of an O + Ne + Mg core," Astrophys. J. **322**, 206 (1987).

[47] S. E. Woosley, A. Heger and T. A. Weaver, "The evolution and explosion of massive stars," Rev. Mod. Phys. **74**, 1015 (2002).

[48] H. Shen, H. Toki, K. Oyamatsu and K. Sumiyoshi, "Relativistic equation of state of nuclear matter for supernova and neutron star," Nucl. Phys. A **637**, 435 (1998) [nucl-th/9805035].

[49] M. Liebendoerfer, O. E. B. Messer, A. Mezzacappa, S. W. Bruenn, C. Y. Cardall and F. K. Thielemann, "A finite difference representation of neutrino radiation hydrodynamics for spherically symmetric general relativistic supernova simulations," Astrophys. J. Suppl. **150**, 263 (2004) [astro-ph/0207036].

[50] T. Totani, K. Sato, H. E. Dalhed and J. R. Wilson, "Future detection of supernova neutrino burst and explosion mechanism," Astrophys. J. **496**, 216 (1998) [astro-ph/9710203].

[51] L. Hudepohl, B. Muller, H. T. Janka, A. Marek and G. G. Raffelt, "Neutrino Signal of Electron-Capture Supernovae from Core Collapse to Cooling," Phys. Rev. Lett. **104**, 251101 (2010) [Erratum-ibid. **105**, 249901 (2010)] [arXiv:0912.0260 [astro-ph.SR]].

[52] G. L. Fogli *et al.*, "Observables sensitive to absolute neutrino masses (Addendum)," Phys. Rev. D **78**, 033010 (2008) [arXiv:0805.2517 [hep-ph]].

[53] T. Schwetz, M. Tortola and J. W. F. Valle, "Global neutrino data and recent reactor fluxes: status of three-flavour oscillation parameters," arXiv:1103.0734 [hep-ph].

[54] B. Dasgupta and A. Dighe, "Collective three-flavor oscillations of supernova neutrinos," Phys. Rev. D **77**, 113002 (2008) [arXiv:0712.3798 [hep-ph]].

[55] H.-T. Janka and W. Hillebrandt, "Monte Carlo simulations of neutrino transport in type II supernovae," Astr. Ap. Suppl. **78**, 375 (1989).

[56] T. Fischer and G. Martínez-Pinedo "Neutrino spectra during the proto-neutron star cooling phase" (in preparation).

[57] D. Autiero *et al.*, "Large underground, liquid based detectors for astro-particle physics in Europe: scientific case and prospects," JCAP **0711**, 011 (2007). [arXiv:0705.0116 [hep-ph]].

[58] M. Wurm *et al.* [LENA Collaboration], "The next-generation liquid-scintillator neutrino observatory LENA," arXiv:1104.5620 [astro-ph.IM].

[59] C. Lunardini and A. Y. Smirnov, "Supernova neutrinos: Earth matter effects and neutrino mass spectrum," Nucl. Phys. B **616**, 307 (2001) [hep-ph/0106149].

[60] A. S. Dighe, M. T. Keil and G. G. Raffelt, "Identifying earth matter effects on supernova neutrinos at a single detector," JCAP **0306**, 006 (2003) [hep-ph/0304150].

[61] B. Dasgupta, A. Dighe and A. Mirizzi, "Identifying neutrino mass hierarchy at extremely small theta(13) through Earth matter effects in a supernova signal," Phys. Rev. Lett. **101**, 171801 (2008) [arXiv:0802.1481 [hep-ph]].

[62] A. S. Dighe, M. T. Keil and G. G. Raffelt, "Detecting the neutrino mass hierarchy with a supernova at IceCube," JCAP **0306**, 005 (2003) [hep-ph/0303210].

[63] K. Abe *et al.* [T2K Collaboration], "Indication of Electron Neutrino Appearance from an Accelerator-produced Off-axis Muon Neutrino Beam," arXiv:1106.2822 [hep-ex].

[64] M. Mezzetto and T. Schwetz, "Theta-13: phenomenology, present status and prospect," J. Phys. G **37**, 103001 (2010) [arXiv:1003.5800 [hep-ph]].

[65] B. Dasgupta, E. P. O'Connor and C. D. Ott, "The Role of Collective Neutrino Flavor Oscillations in Core-Collapse Supernova Shock Revival," arXiv:1106.1167 [astro-ph.SR].

[66] R. F. Sawyer, "The multi-angle instability in dense neutrino systems," Phys. Rev. D **79**, 105003 (2009) [arXiv:0803.4319 [astro-ph]].

[67] L. Scheck, K. Kifonidis, H. T. Janka and E. Mueller, "Multidimensional supernova simulations with approximative neutrino transport. 1. neutron star kicks and the anisotropy of neutrino-driven explosions in two spatial dimensions," Astron. Astrophys. **457**, 963 (2006) [astro-ph/0601302].

[68] H. Duan, G. M. Fuller, J. Carlson and Y. Z. Qian, "Flavor Evolution of the Neutronization Neutrino Burst from an O-Ne-Mg Core-Collapse Supernova," Phys. Rev. Lett. **100**, 021101 (2008) [arXiv:0710.1271 [astro-ph]].

[69] B. Dasgupta, A. Dighe, A. Mirizzi and G. G. Raffelt, "Spectral split in prompt supernova neutrino burst: Analytic three-flavor treatment," Phys. Rev. D **77**, 113007 (2008) [arXiv:0801.1660 [hep-ph]].

[70] J. F. Cherry, G. M. Fuller, J. Carlson, H. Duan and Y. Z. Qian, "Multi-Angle Simulation of Flavor Evolution in the Neutrino Neutronization Burst From an O-Ne-Mg Core-Collapse Supernova," Phys. Rev. D **82**, 085025 (2010) [arXiv:1006.2175 [astro-ph.HE]].